Journal of AgriSearch, 12 (3) : 150-161
An Open Access International Peer Reviewed Quaterly

ISSN : 2348-8808 (Print), 2348-8867 (Online)
https://doi.org/10.21921/jas.v12i03.15245

Drought Trends and Climate Variability in India's Mahi River Basin

Saral Kumar[1], Alok Mishra[1], Anuj Kumar Dwivedi[2*] and Deepak Singh[3]

ABSTRACT

Climate variability and drought have emerged as critical concerns in semi-arid regions, where water resources are acutely sensitive to fluctuations in temperature and precipitation. The Mahi river basin in western India, encompassing Madhya Pradesh, Rajasthan, and Gujarat, has been subject to limited comprehensive long-term studies despite its susceptibility to climate-induced hydrological stress. This study seeks to evaluate long-term trends in climate variables and drought patterns in the Mahi river basin from 1985 to 2022. Utilizing historical climate data and key drought indices Standardized Precipitation Index (SPI), Rainfall Anomaly Index (RAI), and Standardized Anomaly Index (SAI) in conjunction with statistical tools such as Principal Component Analysis (PCA), we assess changes in temperature, precipitation, and drought severity. The results indicate a 1.2°C increase in average annual temperature and significant interannual variability in precipitation, contributing to more frequent and intense drought events. PCA results revealed that SPI and precipitation collectively account for 100% of the variance in drought behavior, underscoring their critical role in drought monitoring. These findings underscore the necessity for adaptive water resource management strategies to enhance resilience in the face of increasing climate variability.

ARTICLE INFO

Received on	:	29/08/2025
Accepted on	:	21/09/2025
Published online	:	30/09/2025

Keywords: Climate variability, Drought indices, Precipitation patterns, Principal component analysis, Water resource management

INTRODUCTION

Droughts are temporary deviations that can occur in various climate zones, unlike the consistently dry conditions typical of regions with low rainfall. These extended dry spells usually arise from a lack of precipitation and gradually affect other parts of the water cycle, causing major impacts on water resources, agriculture, and ecosystems. The Mahi River Basin, which extends across Madhya Pradesh, Rajasthan, and Gujarat, plays a vital role in supporting local livelihoods. However, its water supply is increasingly at risk due to climate variability and frequent droughts. Gaining insight into these changing hydroclimatic patterns is essential for crafting sustainable water management strategies that bolster resilience against the stresses caused by droughts.

Climate variability, which connects short-term weather changes with long-term climate shifts, has led to an increase in the frequency and intensity of extreme events globally, including in India (Scafetta et al., 2017; Masroor et al., 2020; Dutt et al., 2021). The IPCC cautions that global temperatures might rise by 1.5 °C above pre-industrial levels between 2030 and 2052, potentially exacerbating hydrological extremes (Sharma et al., 2018). In this scenario, recent research highlights the critical need to evaluate rainfall variability and drought patterns in Indian basins. Sharma et al. (2022) reported a rise in consecutive dry days, a reduction in wet days, and frequent droughts in the Mahi River Basin using ClimPACT2 indices, SPI, and run theory, pointing to agricultural vulnerabilities. Pawar et al. (2023) utilized long-term station data (1901–2012) with Mann–Kendall, Sen's slope, and ITA tests, uncovering significant spatial differences and seasonal declines but no uniform rainfall trend across the basin. Additionally, Muthiah et al. (2024) assessed both short- and long-term droughts in the Vaippar Basin through SPI and innovative trend analysis, identifying critical rainfall thresholds, recurrence intervals, and drought-prone areas. Together, these studies illustrate that combining long-term datasets, drought indices, and advanced statistical methods is essential for comprehending hydroclimatic variability and informing adaptive water management strategies in India's drought-susceptible basins.

The increasing frequency and severity of extreme weather events, such as droughts, are associated with global climate change. According to the IPCC (2014), the escalation of greenhouse gas emissions is anticipated to intensify warming trends, resulting in significant alterations in precipitation patterns and the hydrological cycle. These climatic changes heighten the probability of extended droughts, thereby

[1]Sam Higginbottom University of Agriculture, Technology & Sciences, Prayagraj- 211007, India
[2]Nation Institute of Hydrology, Roorkee-247667, India
[3]ICAR-Indian Institute of Soil & Water Conservation, Dehradun-248195, India
[*]Corresponding Author E-mail: akdwivedi2009@gmail.com

exacerbating water shortages and adversely affecting agriculture productivity. In semi-arid regions like the Mahi river basin, where precipitation patterns are inherently variable, such climatic uncertainties present a substantial challenge to water resource planning and management (Diffenbaugh and Giorgi, 2012; Dai, 2013).

Precipitation, temperature fluctuations, evapotranspiration rates, and soil moisture levels are critical determinants of water availability (Burke and Brown 2008; Hao and AghaKouchak 2013). This issue is particularly pronounced in regions characterized by high interannual variability in rainfall, where inconsistencies in model outputs complicate the accurate anticipation of future drought conditions (Sohrabi et al., 2015).

Droughts are generally classified into four primary categories: socioeconomic, hydrological, agricultural, and meteorological droughts. Meteorological droughts arise from prolonged periods of insufficient precipitation, while agricultural droughts are characterized by diminished soil moisture levels that impede crop growth (Sun and Yang, 2012). Hydrological droughts occur when extended dry conditions lead to the depletion of groundwater reserves, reservoirs, and river flows, resulting in water scarcity for both domestic and industrial purposes (AghaKouchak et al., 2015; Ahmadalipour et al., 2017). Socioeconomic droughts, considered the most severe, manifest when water shortages disrupt economic activities, food security, and societal stability (Svoboda and Fuchs, 2016). In agricultural regions such as those within the Mahi basin, rainfall constitutes the primary water source for crops, especially in rainfed farming systems. Evapotranspiration, which includes water loss through soil evaporation and plant transpiration, is another critical factor affecting drought severity (Mehran et al., 2015; Xu et al., 2019). Extended periods of below-average rainfall, combined with high evapotranspiration rates, can result in significant soil moisture deficits, negatively impacting crop yields and food security. The capacity of plants to absorb water from the soil largely depends on the availability of moisture in the root zone, making soil water content a vital parameter for assessing agricultural droughts (Trenberth et al. 2014; Xu et al., 2021).

The determination of climate is influenced by several meteorological variables, including temperature, precipitation, atmospheric pressure, wind speed, humidity, and sunshine duration. Climate significantly influences human activities, particularly in sectors such as agriculture, water resources, and health. The increasing global temperature affects the hydrological cycle, resulting in changes in water availability and distribution. These alterations impact not only water resources but also public health, agricultural productivity, and industrial and municipal water demands. Given the close relationship between climate and hydrology, variations in temperature and precipitation are anticipated to modify hydrological variables and increase the frequency of extreme events such as droughts and floods. Monitoring these changes and implementing effective water resource management and climate adaptation strategies are crucial for ensuring food and livelihood security in the context of future climate uncertainty.

In response to the escalating concerns regarding climate change and its effects on the frequency and intensity of droughts, it is imperative to evaluate historical trends and forecast future drought scenarios (Xu et al., 2020). The Mahi river basin, characterized by its reliance on monsoonal rainfall and fluctuating hydrological conditions, serves as an exemplary subject for such an analysis. This study seeks to assess climate variability and drought trends in the Mahi river basin from 1985 to 2022, employing a combination of drought indices, remote sensing datasets, and statistical analyses. By analyzing historical precipitation patterns, temperature trends, and hydrological indicators, this research aims to identify long-term changes in drought characteristics and their potential impacts on water availability and agricultural productivity (Tijdeman et al., 2020; Xu et al., 2019; Lee et al., 2019; Cao et al., 2019). This research contributes to the expanding body of knowledge on climate-induced hydrological risks and highlights the necessity for integrated water resource management strategies. By providing a comprehensive assessment of past and present drought trends in the Mahi River Basin, this study offers valuable insights for policymakers, water managers, and stakeholders involved in sustainable development planning. Addressing the challenges posed by climate variability necessitates a combination of scientific analysis, technological innovation, and policy interventions to ensure long-term water security and resilience in drought-prone regions.

MATERIALS AND METHODS

Study Area

The Mahi river basin encompasses the states of Madhya Pradesh, Rajasthan, and Gujarat, covering an area of 34,842 square kilometers. It is geographically bounded by the Aravalli Hills, Malwa Plateau, Vindhya Range, and the Gulf of Khambhat. The Mahi River, a significant westward-flowing river in India, originates at an elevation of approximately 500 meters near Bhopawar village in the Sardarpur tehsil of Dhar district, Madhya Pradesh. The river traverses a distance of approximately 583 kilometers before discharging into the Arabian Sea via the Gulf of Khambhat. The river system is augmented by key tributaries, including the Som River, which converges from the right, and the Anas and Panam Rivers, which merge from the left. Agricultural land constitutes 63.63% of the basin, while water bodies account for 4.34%. The basin includes 11 parliamentary constituencies (Tijdeman et al.,2020, with 6 located in Gujarat, 3 in Rajasthan, and 2 in Madhya Pradesh. Figure 1 depicts the study area, highlighting the Mahi basin and its network of hydrological observation stations.

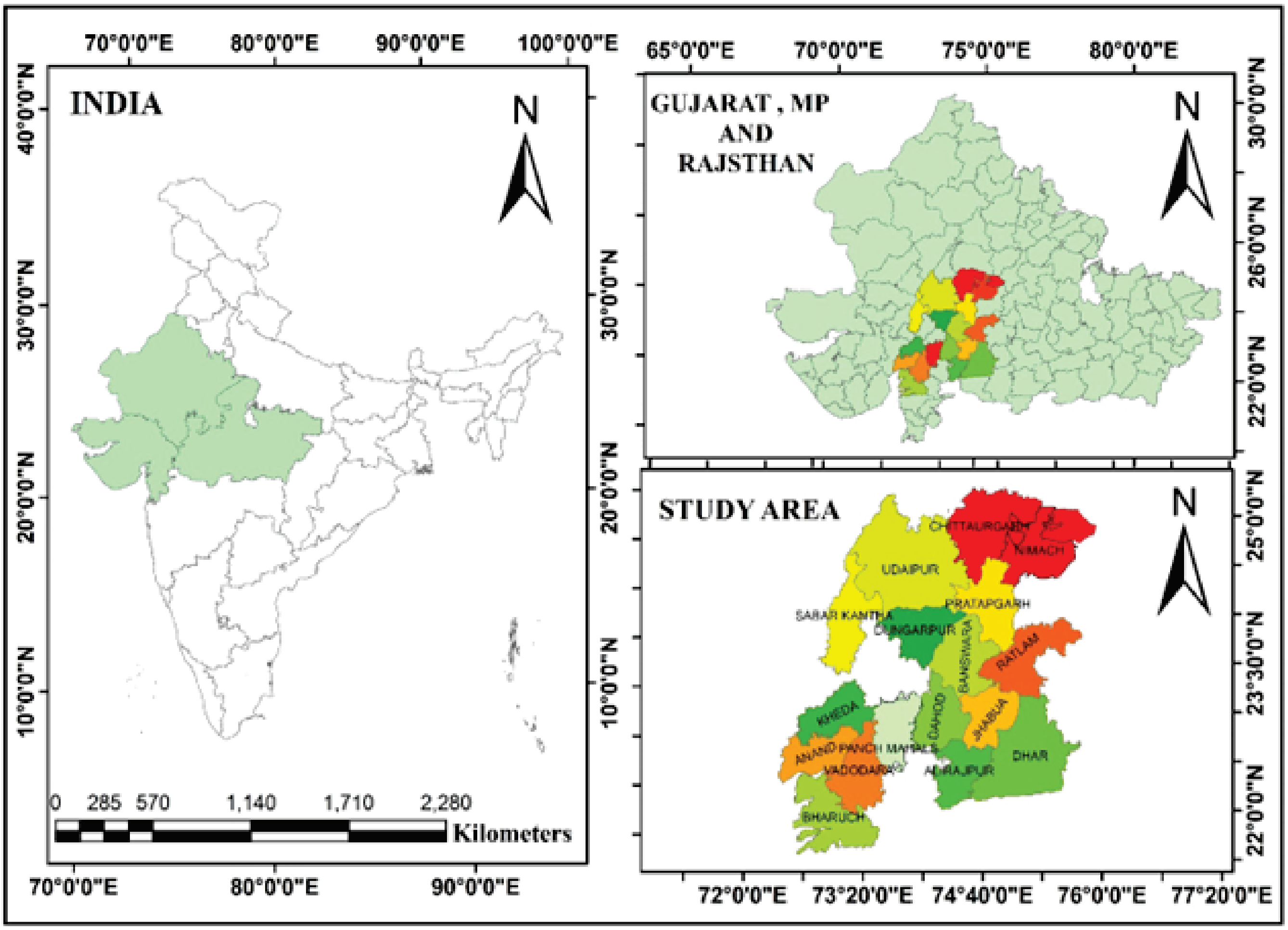

Fig. 1: Study Area

Standardized Precipitation Index (SPI)

The SPI was introduced by McKee et al. (1993) as a drought assessment tool that relies solely on precipitation data, making it computationally efficient with minimal input requirements. This method involves fitting long-term precipitation records from a specific location to a probability distribution.

SPI can be calculated for various time intervals, such as 1 month, 3 months, or even 48 months, allowing it to detect developing drought conditions earlier than the Palmer Drought Severity Index (Palmer, 1965). The ability to analyze precipitation deficits over multiple time scales enables the assessment of their impact on different water resources, including groundwater, soil moisture, reservoir storage, and streamflow.

As a widely used and adaptable drought index, SPI plays a crucial role in identifying and classifying meteorological droughts. Its calculation is based on the Gamma distribution probability density function, represented as follows:

$$g(x) = \frac{1}{\beta^{\alpha}\Gamma(\alpha)} x^{\alpha-1} . e^{\frac{-x}{\beta}} \quad , x > 0 \quad ....(1)$$

Here, $\Gamma(\alpha)$ denotes the gamma function; x represents precipitation (in mm) where (x>0); α is the shape parameter (α>0); and β is the scale parameter (β>0). The classification criteria for SPI values are provided in Table 1.

Table 1: SPI value classification

SPI Value	Class
2.0≥	Extremely Wet
1.5 to 1.99	Very Wet
1.0 to 1.49	Moderately Wet
0.99 to -0.99	Near Normal
-1 to -1.49	Moderately Dry
-1.50 to -1.99	Severely Dry
Below -2.0	Extremely Dry

Standardised Anomaly Index (SAI)

SAI, originally proposed by Kraus in the mid-1970s, was later analyzed in detail by Katz and Glantz at the National Center for Atmospheric Research (NCAR), United States, during the early 1980s. It was developed as an extension of the Rainfall Anomaly Index (RAI), with RAI serving as a fundamental component of SAI. While both indices share similarities, they each possess distinct characteristics, as outlined in Table 2.

$$\text{SAI} = \frac{X-\mu}{\sigma} \quad ....(2)$$

Where,
X=Current Month/Year/Seasonal Rainfall Total(mm)
μ =Mean Annual Rainfall over a period of observation
σ =Standard Deviation of Annual Rainfall over the period of observation

Table 2: Categorization of SAI values

SAI Value	Category
Above 2	Extremely Wet
1.5 to 1.99	Very Wet
1.0 to 1.49	Moderately Wet
-0.99 to 0.99	Near Normal
-1.0 to -1.49	Moderately Dry
-1.5 to -1.99	Severely Dry
-2 or less	Extremely Dry

Rainfall Anomaly Index (RAI)

Van-Rooy introduced the Rainfall Anomaly Index (RAI) in 1965 as a method for assessing precipitation irregularities using a scale ranging from -3 to +3, with 10 predefined bounds. This index relies solely on precipitation data and can be applied at both monthly and annual time scales.

The procedure for calculating RAI involves the following steps:

1. Determine the long-term average monthly precipitation (P) at the selected station.
2. Compute the mean of the 10 highest precipitation values recorded during the statistical period (m).
3. Compute the mean of the 10 lowest precipitation values recorded during the statistical period (X).
4. Compare the monthly precipitation (P) with the long-term mean to assess deviations.

$$\text{RAI} = 3\left[\frac{P-\bar{P}}{\bar{m}-\bar{P}}\right] \quad ....(3)$$

And if P is less than P then RAI is given by

$$\text{RAI} = -3\left[\frac{P-\bar{P}}{\bar{X}-\bar{P}}\right] \quad ....(4)$$

In cases where precipitation deviates from the average, positive anomalies indicate above-normal rainfall, while negative anomalies reflect below-normal rainfall.

5. Set the upper threshold (+3) for the mean of the 10 highest positive anomalies and the lower threshold (-3) for the mean of the 10 lowest negative anomalies.

Table 3 provides a classification of drought severity based on the Rainfall Anomaly Index (RAI).

Table 3: Classification of drought severity by RAI

Category	RAI value
Normal	0 to 3
Weak Drought	-1/0 to 0/3
Moderate Drought	-1/5 to -1/2
Severe Drought	-3 to -1/5
Extreme Drought	Less than -3

RESULTS AND DISCUSSION

Drought severity in this analysis is determined by the threshold-based framework of the Standardized Precipitation Index (SPI) developed by McKee et al. (1993). Within this framework, SPI thresholds between -0.50- and -0.99-mark mild drought, -1.00 to -1.49-mark moderate drought, -1.50 to -1.99 represent severe drought, and values at or below -2.00 indicate extreme drought. For the Rainfall Anomaly Index (RAI), we use the original thresholds set by Van Rooy developed in the year 1965, where RAI values below -1.0 denote significant dry periods and thresholds below -2.0 reflect more severe drought conditions. The Standardized Anomaly Index (SAI), based on Kraus's work in the 1970s, measures deviations from the long-term mean, with thresholds below -1.0 indicating moderate to extreme negative rainfall anomalies. To define drought events more precisely, we adopt a temporal threshold: SPI-based droughts are considered significant if SPI values persist below -1.0 for at least two to three consecutive months, aligning with established drought monitoring standards (). These updated thresholds ensure a clear, scientifically grounded framework for evaluating drought indices and the thresholds applied in this study.

Figure 2 presents the annual precipitation levels, quantified in millimeters (mm), over a 36-year period. The bar graph reveals substantial interannual variability, indicative of fluctuating climatic patterns. The highest precipitation levels were observed in years such as 1995, 2007, and 2021, each exceeding 700 mm. In contrast, years with notably low precipitation, including 1987, 1992, and 2002, recorded less than 300 mm. A discernible pattern of alternating dry and wet years suggests potential cyclical weather patterns or the influence of external climatic phenomena such as El Niño and La Niña. This analysis offers valuable insights for understanding long-term climatic trends and planning for water resource management.

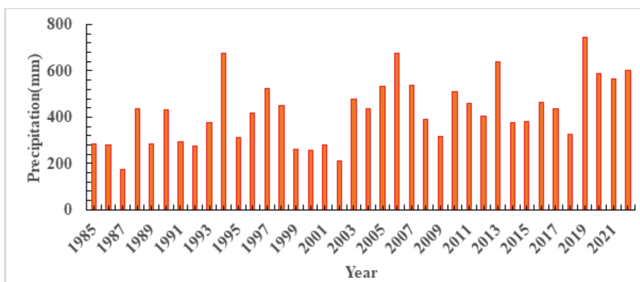

Fig. 2: Annual precipitation trends from 1985-2021

Climate and Drought Dynamics in the Study Region

Figure 3 presents the trends in climate variables and drought indices from 1985 to 2022 for the Mahi River Basin, which encompasses the districts of Madhya Pradesh, Gujarat, and Rajasthan in India. The parameters analyzed include maximum and minimum temperatures, average temperature, average precipitation, relative humidity (RH), and drought indices (RAI, SPI, and SAI). A consistent increase in maximum and average temperatures is observed over the years, indicative of the impacts of rising global warming. The precipitation trend exhibits significant interannual variability, with notable peaks and troughs, suggesting sporadic rainfall events that contribute to fluctuating drought conditions. The drought indices highlight periods of drought severity, with a general upward trend reflecting increased aridity in recent decades. The interplay between temperature, humidity, and precipitation trends underscores the complex nature of climate systems and the potential implications for water availability and agricultural sustainability in the studied region.

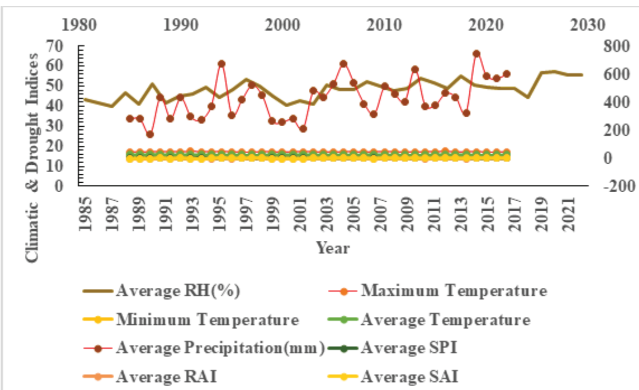

Fig. 3: Trends in Climate Variables and Drought Indices (1985–2022)

Figure 4 depicts the annual fluctuations in the mean Standardized Precipitation Index (SPI), Rainfall Anomaly Index (RAI), and Standardized Anomaly Index (SAI) from 1985 to 2022. These indices collectively elucidate the extent and frequency of drought conditions throughout the observed period. Notably, significant negative values, particularly during the late 1980s, early 1990s, and mid-2000s, indicate periods of severe drought, with SPI and SAI demonstrating a strong correlation in indicating precipitation deficits and broader climatic anomalies. Conversely, maxima in the positive range, notably during the late 1990s and around 2010, suggest periods of excessive rainfall or improved moisture conditions. The persistent fluctuations indicate a dynamic climate system characterized by recurrent drought episodes, interspersed with periods of increased precipitation. These variations underscore the importance of monitoring these indices to anticipate and mitigate drought impacts on agriculture, water resources, and ecosystems. The temporal trend suggests increasing variability, potentially attributable to evolving climatic patterns.

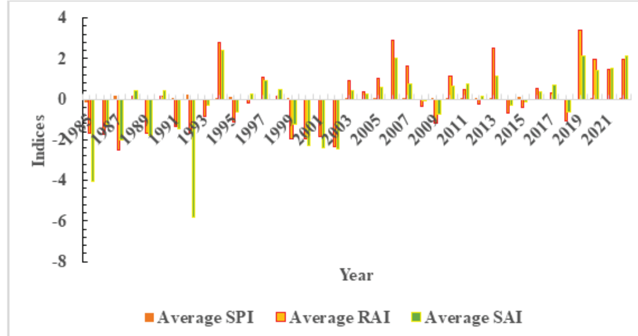

Fig. 4: Yearly Trends in Average SPI, RAI, and SAI Values (1985–2022)

Figure 5 presents a comparative analysis of average relative humidity (RH%) and drought indices (SPI, RAI, and SAI) spanning the period from 1985 to 2022. The data indicate that relative humidity has remained relatively stable over the years, suggesting a limited direct impact of short-term climate variability. Conversely, the drought indices demonstrate significant interannual variability, with marked decreases signifying drought episodes and increases indicating wetter conditions. The alignment of negative indices with lower humidity levels highlights the correlation between diminished atmospheric moisture and the severity of drought conditions. While relative humidity appears more consistent, the variability observed in SPI, RAI, and SAI underscores the intricate interplay of precipitation patterns, temperature, and atmospheric dynamics in influencing drought conditions. These findings underscore the importance of considering multiple indices and climatic parameters for effective drought monitoring and mitigation strategies.

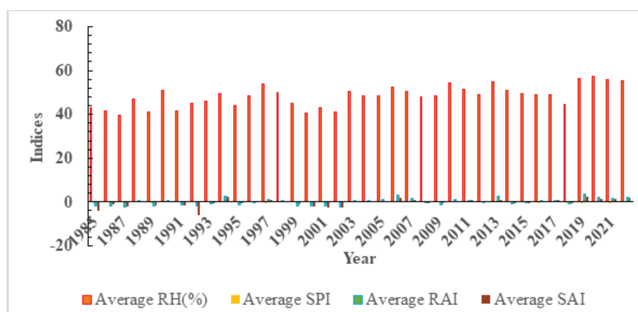

Fig. 5: Temporal Comparison of Average Relative Humidity and Drought Indices (SPI, RAI, SAI) from 1985 to 2022

Figure 6 presents the trends in maximum, minimum, and average temperatures over a 36-year period. The red bars represent maximum temperatures, consistently ranging between 40°C and 50°C, indicating high annual peaks. The yellow bars denote minimum temperatures, generally ranging between 0°C and 20°C, exhibiting considerable variation across the years. The green bars depict average temperatures, which remain relatively stable, fluctuating between 15°C and 30°C. The consistent range of maximum and minimum temperatures suggests a stable thermal amplitude over the years, with no substantial long-term increase or decrease observed. These data underscore the persistence of extreme heat events, which may pose challenges for agriculture, water resource management, and public health. The notable difference between maximum and minimum temperatures emphasizes significant diurnal and seasonal variability, which is critical for understanding local climate dynamics and implementing climate adaptation strategies.

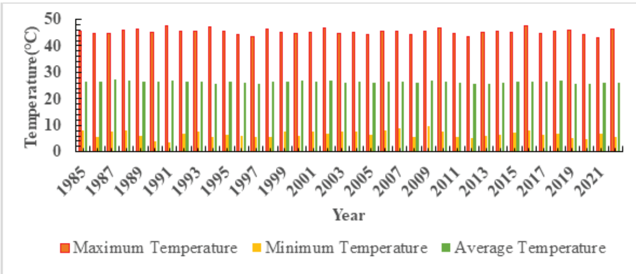

Fig. 6: Annual Temperature Variations of Mahi river basin (1985-2021)

Figure 7 presents the trajectory of the Standardized Precipitation Index (SPI) from 1980 to 2030, elucidating fluctuations in wet and dry conditions over this period. Positive SPI values signify wetter-than-average conditions, whereas negative values indicate drier-than-average periods. The data reveal significant positive SPI peaks in years such as 1997, 1991, and 2013, suggesting extreme wet events, potentially influenced by phenomena such as El Niño. In contrast, notable negative SPI values during the early 1980s and 2010–2020 suggest prolonged drought conditions, with the latter period showing an increased frequency of consecutive dry years, consistent with global trends of intensified drought due to climate change. This variability reflects evolving climate dynamics, where earlier years display more balanced cycles of wet and dry conditions, while the post-2000 period indicates a gradual shift towards more arid conditions. Such trends may have profound implications for water resources, agriculture, and ecosystems, particularly if negative SPI values continue to predominate in the projected future. During the 1980s to mid-1990s, wetter conditions prevailed, with peak SPI values in 1991 (~0.26) suggesting enhanced rainfall likely linked to favorable monsoons. The late 1990s experienced a shift, with 1997 recording a significant drought (SPI ~ -0.18), coinciding with a strong El Niño event. From 2000 to 2010, SPI values remained relatively stable, indicating near-normal rainfall with minimal extremes. However, the period from 2011 onward exhibited increased variability, with alternating dry and wet years, including wetter 2015 and 2021, and drier 2016 and 2018. Overall, the SPI trend reveals a transition from consistently wet conditions to greater climatic variability and drought frequency, underscoring the growing need for proactive drought assessment and adaptive water resource management. The observed extremes highlight the increasing unpredictability of precipitation patterns, necessitating adaptive measures to mitigate the impacts of both drought and excessive rainfall. Understanding these trends is crucial for sustainable water management and developing climate resilience strategies, particularly in regions vulnerable to changing precipitation patterns. Overall, the graph underscores the importance of monitoring SPI as a key indicator of hydrological and climate variability.

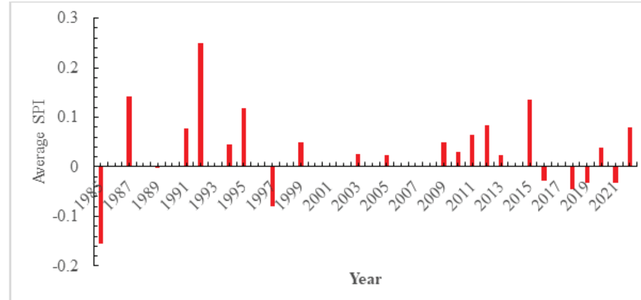

Fig. 7: Trend in Average SPI Over Time (1980-2030)

Figure 8 presents the trend in the Average Rainfall Anomaly Index (RAI) from 1980 to 2030, illustrating temporal variations in precipitation. The RAI measures deviations from average precipitation, with negative values indicating below-average and positive values signifying above-average rainfall conditions. The dotted trendline reveals a slight upward trajectory in rainfall anomalies, as represented by the equation y=0.0733x−146.88 and an R2 value of 0.2656, suggesting a weak positive correlation between time and average RAI. Although the data points display considerable variability, with several extreme positive anomalies (e.g., years of heavy rainfall) and negative anomalies (e.g., drought years), the overall increase in average RAI may suggest a tendency toward wetter conditions in certain periods. However, the relatively low R2 value indicates that the trendline does not fully account for the variability in rainfall anomalies, underscoring the complexity and unpredictability of precipitation patterns. If sustained, this upward trend could indicate shifts in regional climate systems, potentially affecting water resource management and agricultural planning in the future.

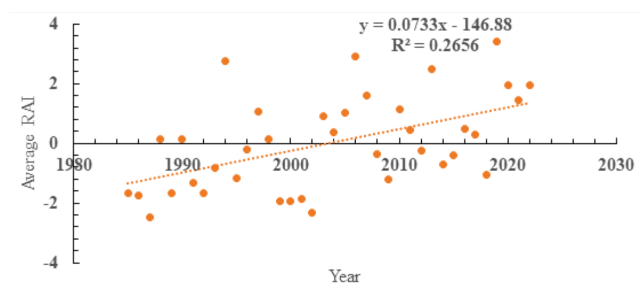

Fig. 8: Trend in Average RAI Over Time (1980-2030)

Figure 9 presents the trend in the Average Standardized Anomaly Index (SAI) from 1980 to 2030, highlighting fluctuations in climate variability. The SAI measures deviations from typical conditions, with positive values indicating wetter or more favorable conditions and negative values signifying drier or adverse anomalies. The dotted trendline shows a slight positive increase over the observed period, represented by the equation y=0.0821x−164.77, with an R2 value of 0.2837. This suggests a weak correlation between time and the SAI, indicating a modest trend towards improving conditions or increased wetness. However, the significant dispersion of data points reveals substantial variability, with extreme negative anomalies observed prior to 2000 and a more frequent clustering of positive anomalies after

2010. The upward trend may reflect long-term shifts in regional climatic patterns, potentially influenced by changes in precipitation or temperature dynamics. While the R2 value suggests limited explanatory power of the trendline, the overall increase in SAI could indicate a gradual progression towards more favorable environmental conditions in certain areas, although the variability underscores the continued unpredictability of climate systems. Understanding these trends is crucial for anticipating potential impacts on agriculture, ecosystems and water resource management.

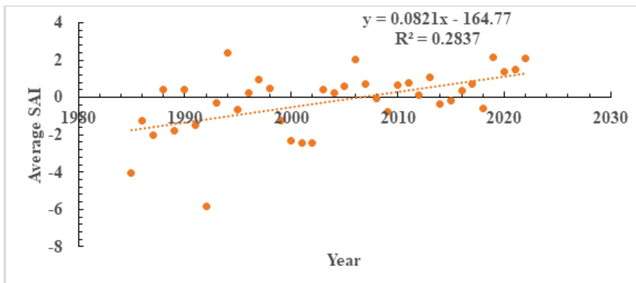

Fig. 9: Trend Analysis of Mean SAI

Fig. 10 illustrates the trend in average relative humidity (RH%) from 1980 to 2030, with data points depicted as orange dots and a fitted linear regression line included. The equation of the trend line is y = 0.2911x - 535, indicating a gradual increase in RH% over the years, with an annual rate of approximately 0.2911% per year. The coefficient of determination ($R^2 = 0.4465$) suggests a moderate correlation between year and average RH%, implying that additional factors may influence the variation. The graph demonstrates a notable upward trend in relative humidity over the observed period.

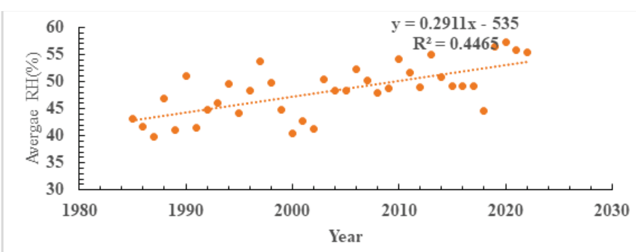

Fig. 10: Trend Analysis of Mean Relative Humidity (%) Over Time

Table 4: Summary of Average Drought Indices (SPI, RAI, SAI) by Year (1985–2022)

Year	Average SPI	Average RAI	Average SAI
1985	-0.15430335	-1.65635213	-4.063449968
1986	-2.48167E-16	-1.726502972	-1.215564583
1987	0.14253104	-2.483162522	-2.008678592
1988	5.48581E-16	0.137890255	0.429346476
1989	-0.000158123	-1.654913313	-1.775568573
1990	-6.26949E-16	0.142876162	0.409310878
1991	0.076902343	-1.323040218	-1.483325074
1992	0.25	-1.665366411	-5.829222011
1993	0	-0.834306412	-0.294269595
1994	0.045661125	2.776192915	2.409209196
1995	0.117608902	-1.152722967	-0.638628984
1996	5.61642E-16	-0.213860034	0.226585586
1997	-0.078903338	1.066733901	0.935920736
1998	-1.09716E-15	0.16021317	0.470965593
1999	0.049525008	-1.932854888	-1.250881653
2000	4.44089E-16	-1.945172877	-2.287259632
2001	-9.63282E-16	-1.873091143	-2.416374121
2002	7.05318E-16	-2.314948797	-2.450669785
2003	0.026159605	0.893151593	0.410576976
2004	0	0.387660113	0.257587306
2005	0.0228039	1.033836439	0.586886719
2006	-3.13475E-16	2.920784041	2.018733315
2007	5.11038E-05	1.609800886	0.719950266
2008	2.15514E-16	-0.36009044	-0.057676381
2009	0.049249225	-1.20592442	-0.752662725
2010	0.029499438	1.131598665	0.641094989
2011	0.065324337	0.458827712	0.766042512
2012	0.084554289	-0.252591748	0.146208458
2013	0.024220185	2.505356832	1.105779908
2014	-1.05798E-15	-0.692814961	-0.321293975
2015	0.134955995	-0.398513888	-0.147666769
2016	-0.028746146	0.504694369	0.366008799
2017	-1.67187E-15	0.287199533	0.707046095
2018	-0.046157216	-1.057543445	-0.613531876
2019	-0.032518269	3.400499679	2.138616107
2020	0.038352677	1.949660453	1.408351036
2021	-0.031608354	1.451167832	1.514981318
2022	0.078812384	1.958170235	2.12421095

The summary presented in Table 4, which details the average drought indices (SPI, RAI, SAI) from 1985 to 2022, reveals a dynamic pattern of drought conditions throughout the study period. Years characterized by significantly negative SPI, RAI, and SAI values, such as 1985, 1992, and 2002, are indicative of severe drought events. In contrast, periods with positive values across these indices, such as 1994, 2006, and 2019, suggest wetter conditions or recovery from drought. Notably, the RAI often exhibits more pronounced fluctuations compared to the SPI and SAI, underscoring its sensitivity to extreme precipitation anomalies. The high positive indices observed in recent years, particularly from 2020 to 2022, imply improved hydrological conditions, potentially influenced by climatic variability or regional interventions. Overall, these trends emphasize the necessity for continuous monitoring and adaptive water resource management to address the variability in drought conditions.

Table 5: Summary statistics Year (1985–2022)

Variable	Observations	Obs. with missing data	Obs. without missing data	Minimum	Maximum	Mean	Std. deviation
Average SPI	38	0	38	-0.154	0.250	0.023	0.067
Average Precipitation (mm)	38	0	38	173.970	743.510	423.438	140.086

Table 5 provides a summary of the statistical characteristics for two primary variables: Average SPI (Standardized Precipitation Index) and Average Precipitation (in mm). The table reveals that there are 38 total observations for both variables, with no missing data. For the Average SPI, the values range from a minimum of -0.154 to a maximum of 0.250, with a mean of 0.023, indicating predominantly neutral conditions concerning precipitation anomalies. The standard deviation for SPI is 0.067, suggesting a moderate degree of variability around the mean. In contrast, the Average Precipitation values exhibit a more extensive range, from 173.970 mm to 743.510 mm, with a mean of 423.438 mm, reflecting substantial variability in precipitation levels across the observations. The standard deviation for Average Precipitation is 140.086 mm, indicating considerable variability in the precipitation amounts observed throughout the study period. These statistics provide a comprehensive overview of the distribution and variability of both precipitation and SPI, offering valuable insights into the hydrological conditions during the study period.

Table 6: Principal Component Analysis (Eigenvalues)

	F1	F2
Eigenvalue	1.198	0.802
Variability (%)	59.899	40.101
Cumulative %	59.899	100.000

Table 6 delineates the outcomes of a Principal Component Analysis (PCA) conducted on the dataset, highlighting the eigenvalues, percentages of variability, and cumulative variability for the initial two principal components (F1 and F2). The eigenvalue for the first principal component (F1) is 1.198, signifying that it accounts for a substantial portion of the total variance in the data, with 59.899% of the total variability explained by this component. The second principal component (F2) possesses an eigenvalue of 0.802, accounting for the remaining 40.101% of the variance. Together, F1 and F2 elucidate 100% of the total variance, affirming that these two components provide a comprehensive representation of the underlying patterns in the dataset. This analysis underscores the importance of dimensionality reduction, as it demonstrates that two principal components suffice to characterize the key variability within the data, which can subsequently be employed for further analysis or visualization. Figure 11 illustrates the eigenvalues for the two principal components (F1 and F2) derived from principal component analysis (PCA), with the left y-axis representing eigenvalues and the right y-axis depicting the cumulative percentage of explained variability. The eigenvalue of F1 exceeds 1.2, indicating that it captures a substantial portion of the dataset's variance, while F2, with an eigenvalue below 1, contributes less significantly. F1 accounts for approximately 60% of the total variability, and the cumulative contribution of both components reaches 100%, fully representing the dataset's variability. The precipitous decline in eigenvalues after F1 underscores diminishing returns in variance explained, consistent with the "elbow criterion" for selecting key components. This analysis is crucial for dimensionality reduction, facilitating efficient data interpretation and feature selection while preserving the majority of the dataset's variability.

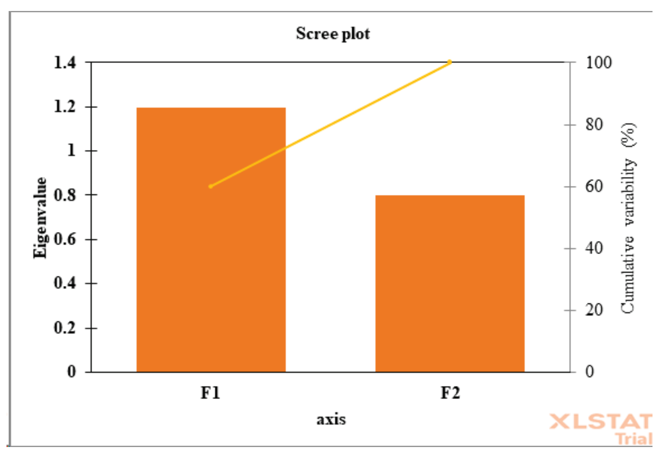

Fig. 11: Relationship Between Eigenvalues and Cumulative Variance in Principal Component Analysis

Table 7: Eigenvectors

	F1	F2
Average SPI	0.707	0.707
Average Precipitation(mm)	-0.707	0.707

Table 7 delineates the eigenvectors corresponding to the first two principal components (F1 and F2) obtained from the Principal Component Analysis (PCA). These eigenvectors reveal the extent to which each variable contributes to the principal components. For F1, both the Average Standardized Precipitation Index (SPI) and Average Precipitation exhibit a value of 0.707, indicating that these variables contribute equally and positively to the first component. This suggests that F1 is significantly influenced by both SPI and precipitation, with these variables demonstrating a positive correlation within the context of this component. In contrast, for F2, the Average SPI is assigned a value of -0.707, whereas Average Precipitation retains a value of 0.707, signifying an inverse relationship. The negative coefficient for SPI and the positive coefficient for precipitation imply that F2 encapsulates the inverse relationship between these variables, where increased precipitation correlates with decreased SPI values (indicative of wetter conditions) and vice versa. These eigenvectors offer valuable insights into the data structure, elucidating the relationships between variables and principal components, thereby facilitating the understanding of underlying patterns within the dataset.

Table 8: Factor loadings

	F1	F2
Average SPI	0.774	0.633
Average Precipitation(mm)	-0.774	0.633

Table 8 presents the factor loadings for the first two principal components (F1 and F2), which represent the relationship between the original variables (Average SPI and Average Precipitation) and the derived factors. The factor loadings indicate the strength of association between each variable and each principal component. For F1, the factor loading for Average SPI is 0.774, and for Average Precipitation, it is -0.774, demonstrating a strong negative correlation between SPI and precipitation within this factor. This suggests that F1 captures the contrast between arid and humid conditions, where higher SPI values (indicating more arid conditions) are associated with lower precipitation values, and vice versa. For F2, both the Average SPI and Average Precipitation have factor loadings of 0.633, indicating a moderate positive relationship between these variables and F2. This suggests that F2 reflects a less extreme, more balanced relationship where both SPI and precipitation are positively correlated, albeit to a lesser extent than in F1. These factor loadings facilitate the interpretation of the underlying patterns represented by the principal components and provide insights into the interaction between precipitation and SPI within the dataset.

Table 9: Correlations between variables and factors

	F1	F2
Average SPI	0.774	0.633
Average Precipitation(mm)	-0.774	0.633

Table 9 delineates the correlations between the original variables, namely Average SPI and Average Precipitation, and the two principal components, F1 and F2. These correlations elucidate the magnitude and direction of the relationship between each variable and the derived factors. For F1, the correlation between Average SPI and F1 is 0.774, whereas the correlation between Average Precipitation and F1 is -0.774, indicating a strong negative relationship. This suggests that F1 encapsulates the inverse relationship between SPI and precipitation, with higher SPI values (indicative of more arid conditions) associated with lower precipitation, and vice versa. Conversely, for F2, both Average SPI and Average Precipitation exhibit a correlation of 0.633, indicating a moderate positive relationship. This implies that F2 represents a scenario where both variables tend to increase or decrease concomitantly, with higher precipitation associated with higher SPI values (indicative of more humid conditions). These correlations provide valuable insights into how the original variables contribute to the principal components and facilitate the understanding of the underlying patterns of variability in the dataset.

Figure 12 presents a biplot that delineates the relationship between average precipitation (mm) and the Standardized Precipitation Index (SPI) along two principal components, F1 (59.90%) and F2 (40.10%), which together account for the entirety of the variance. The average SPI demonstrates a strong association with F1, indicating its significant contribution to the primary source of variation. In contrast, average precipitation is more closely aligned with F2, suggesting its predominant role in explaining the secondary component of variability. The near-orthogonal relationship between these two variables implies a low correlation within the dataset. This observation highlights that while SPI and precipitation are related to hydrological conditions, they capture distinct dimensions of variability, thereby underscoring the importance of both metrics in comprehensive drought analysis.

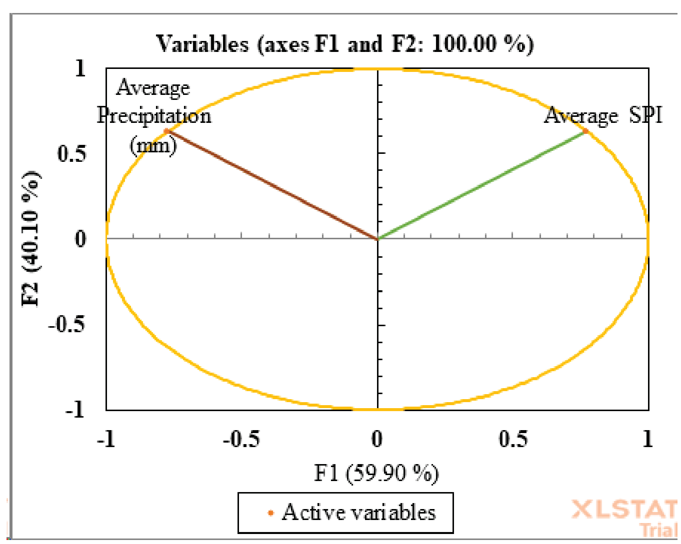

Fig. 12: Biplot Analysis of Average Precipitation and SPI on Principal Components F1 and F2

Table 10: Contribution of the variables (%)

	F1	F2
Average SPI	50.000	50.000
Average Precipitation(mm)	50.000	50.000

Table 10 delineates the contribution of each variable to the two principal components (F1 and F2), with the percentages indicating the extent to which each variable contributes to the overall variance explained by the components. For both F1 and F2, the contributions of Average SPI and Average Precipitation are equally distributed, with each variable contributing 50% to the respective component. This indicates that both variables play an equivalent and significant role in defining the structure of each principal component. Specifically, F1 is composed of an equal combination of Average SPI and Average Precipitation, while F2 also reflects an equal influence of both variables. The equal distribution of contributions suggests that both SPI and precipitation are key factors in elucidating the variability captured by the principal components, and there is no predominance of one variable over the other in shaping the principal components. This balanced contribution underscores the interrelationship between these variables and their joint influence on the underlying patterns of the data.

Figure 13 presents the distribution of observations based on their projections onto two principal components: F1, which accounts for 59.90% of the variance, and F2, which explains 40.10%, collectively representing the entirety of the total variability. The observations are widely dispersed across the four quadrants, indicating heterogeneity in the patterns captured by the two components. Observations such as Obs3 and Obs38 are positioned at the extremes, suggesting they exert significant influence in defining the variability along F1 and F2, respectively. Observations clustered near the origin (e.g., Obs18, Obs16, and Obs90) exhibit minimal contributions to variability, indicating similar characteristics among these data points. The graphical representation aids in identifying outliers, clusters, and patterns within the dataset, highlighting the utility of Principal Component Analysis (PCA) in elucidating underlying structures and relationships among the observations.

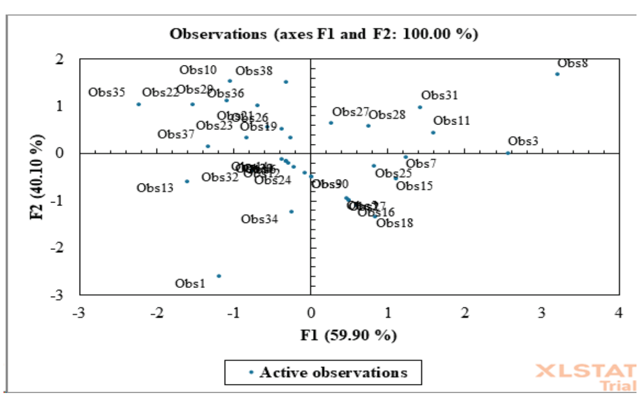

Fig. 13: Principal Component Analysis: Projection of Observations on Components F1 and F2

Figure 14 depicts the relationship between two principal components, F1 (59.90%) and F2 (40.10%), which together account for the entirety of the variability in the dataset. F1 shows a strong association with "Average SPI," as indicated by its pronounced vector alignment along the positive F1 axis, whereas F2 is correlated with "Average Precipitation (mm)," with its vector predominantly aligned along the positive F2 axis. Observations such as Obs3, Obs8, and Obs11 correspond to elevated values of "Average SPI," while Obs10 and Obs38 are linked to higher "Average Precipitation (mm)." Observations in the negative F1 or F2 regions, such as Obs1 and Obs13, exhibit opposing trends. The orthogonal arrangement of the vectors suggests minimal correlation between the two variables. This biplot serves as an effective tool for elucidating patterns, clustering, and variable importance, thereby facilitating the interpretation of multivariate data in hydrological or environmental research.

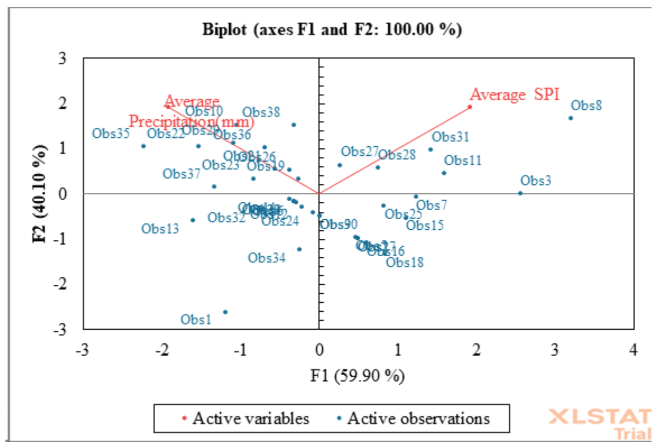

Fig. 14: Biplot Representation of Principal Components (F1 and F2) with Active Variables and Observations

Table 11: Axes homogeneity index:

	Value
F1	0.289
F2	0.395

Table 11 presents the Axes Homogeneity Index (AHI) for the first two principal components (F1 and F2), which quantifies the degree of homogeneity or the extent to which each component effectively captures a uniform structure within the data. The AHI values for F1 and F2 are 0.289 and 0.395, respectively, indicating moderate homogeneity for both components. A lower AHI value suggests that F1 and F2 exhibit relatively less consistent or more varied contributions from the variables involved, implying that these components may represent diverse patterns or factors within the data. Specifically, the higher value for F2 (0.395) suggests that this component may encompass a broader range of variation or more complex relationships compared to F1, which has a slightly lower value of 0.289. The AHI values thus provide insight into the efficacy of each principal component in capturing a coherent structure of the data, with both components demonstrating moderate, but not optimal, homogeneity in the relationships they represent.

Figure 15 presents the homogeneity index values for the two principal components, F1 and F2, which reflect their consistency and representativeness in elucidating the dataset's structure. F2 exhibits a higher homogeneity index, surpassing 0.4, indicating a greater uniformity in its contribution to the dataset's variability. Conversely, F1 possesses a lower homogeneity index, approximately 0.3, suggesting relatively less structural coherence. The greater homogeneity of F2 underscores its reliability in capturing stable patterns within the data, whereas the slightly lower homogeneity of F1 may be influenced by the presence of more diverse or less correlated variables. Collectively, these findings highlight the complementary roles of F1 and F2 in representing the dataset, emphasizing the importance of considering both variance and homogeneity when selecting principal components for applications such as clustering, classification, or dimensionality reduction.

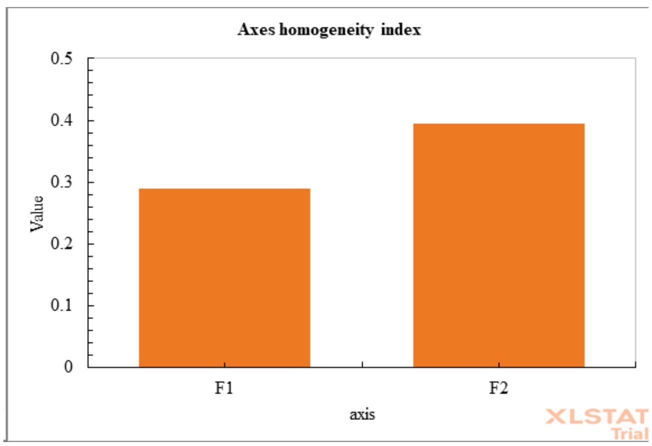

Fig. 14: Homogeneity Index Analysis on Principal Component Axes F1 and F2

CONCLUSION

The study of climate variability and drought patterns in the Mahi River Basin from 1985 to 2022 indicates a 1.2 °C increase in average temperature, coupled with highly unpredictable rainfall ranging from less than 400 mm during drought years to over 1,000 mm in wetter periods, which has heightened evapotranspiration and water stress. Drought indices such as SPI, RAI, and SAI effectively captured these extremes, with SPI falling below –1.5 in severe droughts and rising above +2.0 in wet periods, while RAI and SAI showed slight increases after 2010 despite ongoing variability. Principal Component Analysis (PCA) demonstrated that SPI and precipitation together account for 100% of the variance (F1 = 59.9%, F2 = 40.1%), with SPI closely associated with drought severity and precipitation indicating broader hydrometeorological changes. The orthogonal relationship between these variables emphasizes their complementary roles in monitoring drought dynamics. These results highlight the importance of combining robust drought indices with multivariate tools like PCA to enhance adaptive water management and resilience planning in drought-prone areas.

ACKNOWLEDGEMENTS

The author thanks to the dean Vaugh Institute of Engineering & Technology, SHUATS-Allahabad for providing necessary facility to conduct the research work.

CONFLICT OF INTEREST

The authors declare there is no conflict.

REFERENCES

AghaKouchak A, Farahmand A, Melton F S, Teixeira J, Anderson M C, Wardlow B D and Hain C R. 2015. Remote sensing of drought: Progress, challenges and opportunities. Reviews of Geophysics 53(2): 452–480.

Ahmadalipour A, Moradkhani H, Yan H and Zarekarizi M. 2017. Remote sensing of drought: Vegetation, soil moisture, and data assimilation. In Remote Sensing of Hydrological Extremes (pp. 121–149).

Burke E J and Brown S J. 2008. Evaluating uncertainties in the projection of future drought. Journal of Hydrometeorology 9(2): 292–299.

Cao Y, Chen S, Wang L, Zhu B, Lu T and Yu Y. 2019. An agricultural drought index for assessing droughts using a water balance method: A case study in Jilin Province, Northeast China. Remote Sensing 11(9): 1066.

Dai A. 2013. Increasing drought under global warming in observations and models. Nature Climate Change 3(1): 52–58.

Diffenbaugh N S and Giorgi F. 2012. Climate change hotspots in the CMIP5 global climate model ensemble. Climatic Change 114: 813–822.

Dutt S, Gupta A K, Cheng H, Clemens S C, Singh R K and Tewari V C. 2021. Indian summer monsoon variability in northeastern India during the last two millennia. Quaternary International 571: 73-80.

Hao Z and AghaKouchak A. 2013. Multivariate standardized drought index: A parametric multi-index model. Advances in Water Resources 57: 12–18.

IPCC. 2014. Climate Change 2014: Synthesis Report. Contribution of Working Groups I, II, and III to the Fifth Assessment Report of the Intergovernmental Panel on Climate Change. IPCC, Geneva, Switzerland, 151 pp.

Lee M H, Im E S and Bae D H. 2019. A comparative assessment of climate change impacts on drought over Korea based on multiple climate projections and multiple drought indices. Climate Dynamics 53: 389–404.

Masroor M, Rehman S, Avtar R, Sahana M, Ahmed R and Sajjad H. 2020. Exploring climate variability and its impact on drought occurrence: Evidence from Godavari Middle sub-basin, India. Weather and Climate Extremes 30: 100277.

McKee T B, Doesken N J and Kleist J. 1993. The relationship of drought frequency and duration to time scales. In Proceedings of the 8th Conference on Applied Climatology (Vol. 17, No. 22, pp. 179–183).

Mehran A, Mazdiyasni O and AghaKouchak A. 2015). A hybrid framework for assessing socioeconomic drought: Linking climate variability, local resilience, and demand. Journal of Geophysical Research:

Atmospheres 120(15): 7520–7533.

Muthiah M, Sivarajan S, Madasamy N, Natarajan A and Ayyavoo R. 2024. Exploring short-and long-term meteorological drought parameters in the Vaippar Basin of Southern India. Scientific Reports 14(1): 13428.

Palmer W C. 1965. Meteorological drought (Vol. 30). US Department of Commerce, Weather Bureau.

Pawar U, Hire P, Gunathilake M B and Rathnayake U. 2023. Spatiotemporal rainfall variability and trends over the Mahi basin, India. Climate 11(8): 163.

Scafetta N, Mirandola A and Bianchini A. 2017. Natural climate variability, part 1: Observations versus the modeled predictions. International Journal of Heat and Technology 35(S1): S9-S17.

Sharma A, Sharma D and Panda S K. 2022. Assessment of spatiotemporal trend of precipitation indices and meteorological drought characteristics in the Mahi River basin, India. Journal of Hydrology 605: 127314.

Sharma A, Sharma D, Panda S K, Dubey S K and Pradhan R K. 2018. Investigation of temperature and its indices under climate change scenarios over different regions of Rajasthan state in India. Global and Planetary Change 161: 82-96.

Sohrabi M M, Ryu J H, Abatzoglou J and Tracy J. 2015. Development of soil moisture drought index to characterize droughts. Journal of Hydrologic Engineering 20(11): 04015025.

Sun C and Yang S. 2012. Persistent severe drought in southern China during winter–spring 2011: Large-scale circulation patterns and possible impacting factors. Journal of Geophysical Research: Atmospheres 117(D10).

Svoboda M D and Fuchs B A. 2016. Handbook of drought indicators and indices (Vol. 2). Geneva, Switzerland: World Meteorological Organization.

Tijdeman E, Stahl K and Tallaksen L M. 2020. Drought characteristics derived based on the standardized streamflow index: A large sample comparison for parametric and nonparametric methods. Water Resources Research 56(10): e2019WR026315.

Trenberth K E, Dai A, Van Der Schrier G, Jones P D, Barichivich J, Briffa K R and Sheffield J. 2014. Global warming and changes in drought. Nature Climate Change 4: 17–22.

Xu L, Abbaszadeh P, Moradkhani H, Chen N and Zhang X. 2020. Continental drought monitoring using satellite soil moisture, data assimilation and an integrated drought index. Remote Sensing of Environment 250: 112028.

Xu L, Chen N and Zhang X. 2019. Global drought trends under 1.5 and 2°C warming. International Journal of Climatology 39(4): 2375–2385.

Xu L, Chen N, Zhang X, Moradkhani H, Zhang C and Hu C. 2021. In-situ and triple-collocation based evaluations of eight global root zone soil moisture products. Remote Sensing of Environment 254: 112248.

Citation:
Kumar S, Mishra A, Dwivedi A K and Singh D.2025. Drought trends and climate variability in India's Mahi river basin. Journal of AgriSearch 12(3): 150-161.